Semi-Continuity of Skeletons in 2-Manifold and Discrete Voronoi Approximation

Yong-Jin Liu, *Member, IEEE*

Abstract—The skeleton of a 2D shape is an important geometric structure in pattern analysis and computer vision. In this paper we study the skeleton of a 2D shape in a 2-manifold $\mathcal{M}$, based on a geodesic metric. We present a formal definition of the skeleton $S(\Omega)$ for a shape Ω in $\mathcal{M}$ and show several properties that make $S(\Omega)$ distinct from its Euclidean counterpart in $\mathbb{R}^2$. We further prove that for a shape sequence $\{\Omega_i\}$ that converge to a shape Ω in $\mathcal{M}$, the mapping $\Omega \to \overline{S}(\Omega)$ is lower semi-continuous. A direct application of this result is that we can use a set P of sample points to approximate the boundary of a 2D shape Ω in $\mathcal{M}$, and the Voronoi diagram of P inside $\Omega \subset \mathcal{M}$ gives a good approximation to the skeleton $S(\Omega)$. Examples of skeleton computation in topography and brain morphometry are illustrated.

Index Terms—2D shape sequence, Voronoi skeleton, 2-manifold, geodesic.

1 Introduction

The skeleton of a 2D shape is an important geometric structure which has found a wide range of applications in pattern analysis and computer vision. Many previous works focus on the skeleton of a shape defined in a Euclidean space, such as a 2D shape in the plane $\mathbb{R}^2$ and a 3D solid in $\mathbb{R}^3$. In recent years, the study of 2D shapes in a general 2-manifold $\mathcal{M}$ has received increased attention for many applications; e.g., (1) 2D shapes in images that are embedded as 2-manifolds in various high-dimensional spaces for geometric flow analysis of images [14]; (2) 2D shapes such as ridge, basin and lake regions in a terrain domain (Figure 1) for motion planning [13]; (3) sulcal and gyral regions on cortical surfaces for medical image analysis [31].

In this paper, we study the skeleton of a 2D shape defined in $\mathcal{M}$ based on a geodesic metric. There are several closely related terms of skeletons in literature, including medial axis [4], shock graph [12], [34] and cut locus [37], [38]. For a 2D shape Ω in the plane $\mathbb{R}^2$, the *skeleton* is the set of centers of maximal open disks contained in Ω [24], [28]; the *medial axis* is the set of points in Ω which have at least two closest points in $\mathbb{R}^2 \setminus \Omega$ and is always a subset of the skeleton [4], [28]; the *shock graph* is a directed, acyclic graph of shock groups where the loci of shock positions are the medial axis [12], [34]; the *cut loci* is the closure of the set containing all points which have at least two closest paths to the boundary of Ω [37]. Based on a geodesic metric, we present a formal definition of the skeleton of a 2D shape in $\mathcal{M}$ in Section 4.

The challenge of defining and studying the skeleton of a 2D shape in $\mathcal{M}$ stems from the geodesic metric d_g. For example, the skeleton definition in $\mathbb{R}^2$ relies on an open disk which is always bounded by a planar circle. However, only if a radius r is smaller than the injectivity radius at a $p \in \mathcal{M}$, a geodesic disk $D_r(p) = \{q \in \mathcal{M} | d_g(p,q) < r\}$ is homeomorphic to a planar disk [6]. It was shown in [20] that in $\mathcal{M}$ of genus g, the boundary of $D_r(p)$ can have up to $g+1$ separated closed curves. In this paper we further show that, distinct from its Euclidean counterparts, the skeleton of a shape that encloses a connected region in $\mathcal{M}$ can be disconnected.

In this paper we study a mapping S from a given 2D shape $\Omega \subset \mathcal{M}$ to a skeleton $S(\Omega) \subset \mathcal{M}$ and prove the following result: For a shape sequence $\{\Omega_i\}$ converging to a shape Ω in $\mathcal{M}$, the mapping from $\{\Omega_i\}$ to $\{S(\Omega_i)\}$ is lower semi-continuous. A direct application of this result is

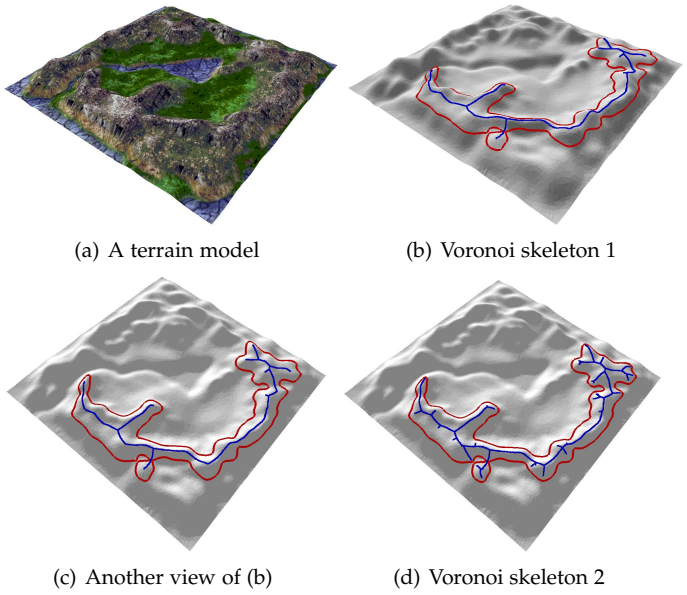

(a) A terrain model (b) Voronoi skeleton 1 (c) Another view of (b) (d) Voronoi skeleton 2

Fig. 1. Skeletons on a 2-manifold $\mathcal{M}$. A stratigraphic ridge Ω in $\mathcal{M}$ is bounded by a red curve (having the same altitude) and the skeleton of Ω is shown in blue. Voronoi skeletons 1 and 2 are at granularities 20 and 3 (detail about granularity is presented in Section 6.2).

• *Y.J. Liu is with Tsinghua National Laboratory for Information Science and Technology, the Department of Computer Science and Technology, Tsinghua University, Beijing, China.*
E-mail: liuyongjin@tsinghua.edu.cn

that we can sample the boundary of Ω using a sequence of dense sample points $\{P_i\}$, then the Voronoi diagrams $\{V(P_i)\}$ inside $\Omega \subset \mathcal{M}$ give good approximations to the skeleton $S(\Omega)$. The 2-manifold $\mathcal{M}$ studied in this paper is general, i.e., either a smooth surface with bounded principal curvatures or a piecewise linear surface (e.g., a 2-manifold triangular or quadrilateral mesh) embedded in $\mathbb{R}^n, n \geq 3$.

2 Related Work

The medial axis or the skeleton of a shape in Euclidean spaces has attracted considerable attention in computer vision and pattern analysis [33]. Lieutier [18] proved that any bounded open subset $O \subset \mathbb{R}^n$ has the same homotopy type as its medial axis. The stability of the medial axis and skeleton of O have been investigated in [7], [8]. An elegant λ-medial axis was further proposed in [9], showing that for regular values of λ, the λ-medial axis remains stable under Hausdorff distance perturbations of O. All these works focus on the domain of open subsets in $\mathbb{R}^n$. In this paper, we study the convergence of skeletons of open subsets in a 2-manifold $\mathcal{M}$ based on a geodesic metric.

For any two points p and q in $\mathcal{M}$, the shortest path joining p and q is a geodesic. The Hopf-Rinow theorem [6] for smooth surfaces and its adaption [1] to piecewise linear surfaces ensure that a geodesic always exists for any two points in $\mathcal{M}$. The geodesic offers a metric d_g in $\mathcal{M}$, such that $\forall p, q \in \mathcal{M}$, the geodesic distance $d_g(p, q)$ is the length of the shortest path in $\mathcal{M}$ joining p and q. Wolter [37] studied the geodesic metric in a bordered Riemannian manifold and showed that, the geodesic distance function $d_g(A, \cdot)$ to a closed set $A \subset \mathcal{M}$ is C^1-smooth in the complement of C_A in $M \setminus (\partial\mathcal{M} \cup A)$, where C_A is the cut loci of A and $\partial\mathcal{M}$ is the boundary of $\mathcal{M}$. For piecewise linear surfaces, the geodesic metric was studied in [19], [25], which shows $d_g(A, \cdot)$ is uniformly Lipschitz continuous.

Numerical methods had been proposed for computing geodesics in both smooth parametric surfaces [22] and piecewise linear surfaces [15], [25]. Geodesic-based distance functions in $\mathcal{M}$ can be characterized by level sets or equivalent iso-contours. The structure of iso-contours in piecewise linear surfaces was studied in [20]. By regarding piecewise linear surfaces as linear approximations of smooth 2-manifolds, the fast marching [29] and level set methods [27], [30] by solving the Eikonal equation in 2-manifold meshes have been studied. Shi et al. [31] extended the method of Hamilton-Jacobi skeleton [32] from a Euclidean plane to a piecewise linear surface, and its application in medical image analysis was also presented in [31].

Some researchers studied the geometric properties related to skeletons in $\mathcal{M}$. Notably, Wolter [37] studied the cut loci and used it to characterize the regularity of a geodesic distance function $d_g(A, \cdot)$ in general Riemannian manifolds. Lai [16] systematically investigated the variational problem with Laplace-Beltrami eigen-geometry in 2D smooth surfaces and showed that a novel skeleton of a subset in a smooth 2-manifold can be obtained from Reeb graphs. In this paper, we study the convergence of skeletons of a shape sequence in a general 2-manifold $\mathcal{M}$, and show that the Voronoi diagram of dense sampling of the shape boundary can well approximate the skeleton of the shape. For 2-manifold triangular meshes, the exact geodesic [19], [25], [36] and Voronoi diagram [20] can be computed efficiently using computational geometry methods. As a comparison, the numerical solutions of the Hamilton-Jacobi equation or Laplace-Beltrami operator may be sensitive to the triangular shape and triangle density of the mesh.

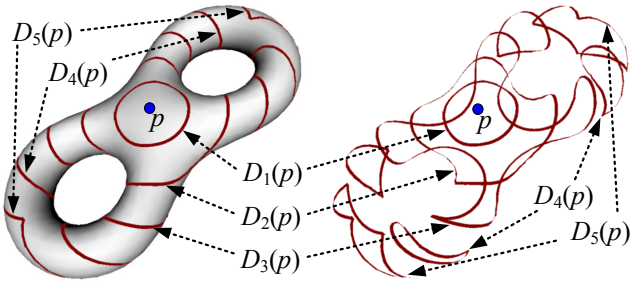

Fig. 2. Geodesic disks $D_r(p)$ in $\mathcal{M}$: disks of $r = 1, 2, 3$ are homeomorphic to a planar disk while disks of $r = 4, 5$ are not.

3 Preliminary on Hit or Miss Topology

Let $\mathcal{M}$ be a connected, closed 2-manifold[1]. Ω is a bounded and connected 2D region in $\mathcal{M}$. $\partial\Omega = \overline{\Omega} \cap \overline{(\mathcal{M} \setminus \Omega)}$ is the boundary of Ω. Based on the geodesic metric d_g in $\mathcal{M}$, a geodesic r-disk centered at a $p \in \mathcal{M}$ is defined by

$$D_r(p) = \{q \in \mathcal{M} | d_g(p, q) < r\}. \quad (1)$$

Whenever there is no risk of confusion, we omit the term "geodesic" and simply call D_r an r-disk. An r-disk in $\mathcal{M}$ may not be homeomorphic to a planar disk (Figure 2).

A set $U \subset \mathcal{M}$ is open if and only if $\forall p \in U, \exists \delta > 0$ such that $D_\delta(p) \subset U$. Let $\mathcal{O}$ be the collection of all the open sets in $\mathcal{M}$ and $\mathcal{C} = \{\mathcal{M} \setminus o | o \in \mathcal{O}\}$ be the collection of all the closed sets in $\mathcal{M}$. The empty set $\emptyset$ and $\mathcal{M}$ are both open and closed.

Let $\mathcal{X} \in \{\mathcal{O}, \mathcal{C}\}$. $\mathcal{X}$ can be regarded as a space X in which the "points" are sets in $\mathcal{M}$. A hit or miss topology [23], [28] is defined on $\mathcal{X}$ using a definition of neighborhoods[2], which consist of packed points in the space X equivalent to a collection of sets in $\mathcal{M}$.

The main result in the hit or miss topology that we use in this paper follows.

Definition 1. *[28] Let I be an index set. A sequence $\{x_i\}, i \in I$, converge to x in $\mathcal{X}$ if and only if it satisfies two conditions:*

1) *If an open set o intersects x, then there exists an n such that o intersects all the $x_i, \forall i > n$.*
2) *If a closed set c is disjoint from x, then there exists an m such that c is disjoint from all the $x_i, \forall i > m$.*

x is called the limit of this sequence, written as $lim\{x_i\} = x$.

1. A closed manifold is a compact manifold without boundary.

2. Formally, given two finite sequences $O = \{o_1, \cdots, o_i, \cdots, o_m\}$ of open sets and $C = \{c_1, \cdots, c_j, \cdots, c_n\}$ of closed sets in $\mathcal{M}$, the collection of all the elements in $\mathcal{X}$ which intersect every o_i and are disjoint from every c_j defines an open (O, C)-neighborhood in $\mathcal{X}$ [23], [28]. Note that in the general hit or miss topology, C is a sequence of compact sets. In this study, the space $\mathcal{M}$ is always bounded and we directly use the terminology of closed sets.

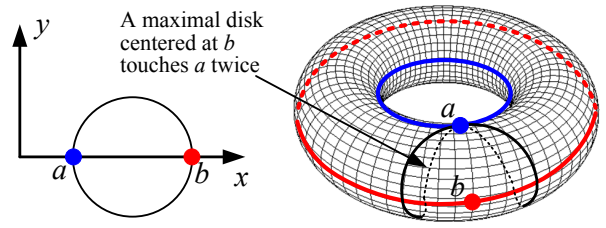

Fig. 3. A skeleton does not have medial axis points. Place a circle in the coordinate system as shown in left and $\overline{ab}$ is a diameter of the circle in x-axis. Rotate the circle around y-axis to get a torus $\mathcal{M}$, and a is rotated into a circle C_{blue} and b into a circle C_{red}. C_{red} is the skeleton of open set $\mathcal{M} \setminus C_{blue}$ and C_{red} has no medial axis points. Centered at each point in C_{red}, there is a maximal disk whose boundary touches only one point in C_{blue} twice.

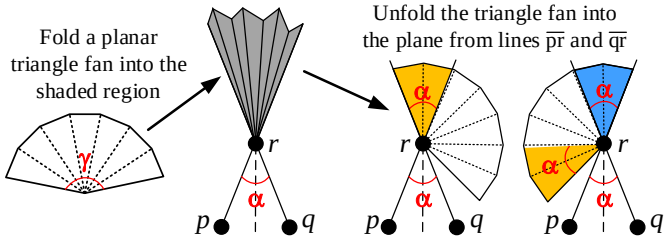

Fig. 4. 2D bisector. r lies on the bisector of points p and q in $\mathbb{R}^2$ and $\angle prq = \alpha$. A planar triangle fan with a spanning angle $\gamma > 2\alpha$ is folded into the gray-shaded area (middel left). When unfolding the triangle fan from the lines $\overline{pr}$ and $\overline{qr}$, respectively, inside the triangle fan, the yellow (or blue) region has a shorter geodesic distance to point p (or q), and the uncolored area with a spanning angle $\gamma - 2\alpha$ has equal geodesic distance to both p and q.

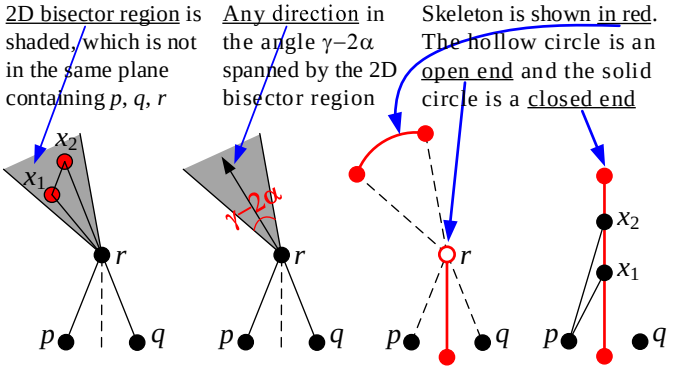

Fig. 5. A disconnected skeleton in $\mathcal{M}$ and a connected skeleton in $\mathbb{R}^2$. See text for full description.

4 Skeleton of An Open Set in $\mathcal{M}$

Matheron [24] chose to define the skeleton in $\mathbb{R}^2$ using open sets due to the reason that the closure of the skeleton is connected if the planar shape is connected[3]. We follow [24] to use open sets for defining the skeleton in $\mathcal{M}$.

Denote by $\mathcal{D}$ the collection of all r-disks $D_r(p) \subset \mathcal{M}$, $\forall p \in \mathcal{M}$ and $r > 0$. Based on the geodesic metric $d_g(\cdot)$ in $\mathcal{M}$, we have

Property 1. *$D_{r_1}(p_1) \subset D_{r_2}(p_2)$ if and only if $d_g(p_1, p_2) \leq r_2 - r_1$.*

Proof. $\forall q \in D_{r_1}(p_1)$, $d_g(q, p_2) \leq d_g(q, p_1) + d_g(p_1, p_2)$. Since q can be chosen arbitrarily, $d_g(q, p_2)$ can reach $r_1 + d_g(p_1, p_2)$. If $D_{r_1}(p_1) \subset D_{r_2}(p_2)$, then $d_g(q, p_2) < r_2$. Thus $d_g(p_1, p_2) \leq r_2 - r_1$. On the other hand, if $d_g(p_1, p_2) \leq r_2 - r_1$, then $r_2 \geq r_1 + d_g(p_1, p_2) > d_g(q, p_1) + d_g(p_1, p_2) \geq d_g(q, p_2)$ and thus $q \in D_{r_2}(p_2)$. □

The relation "is a proper subset of" is a strict partial order on $\mathcal{D}$. By Zorn's lemma [26], we have:

Property 2. *Any disk in a subset of $\mathcal{D}$ is contained in a maximal disk in that subset.*

Definition 2. *Let Ω be an open set in $\mathcal{M}$. The skeleton of Ω, denoted by $S(\Omega)$, is the set of centers of maximal geodesic open disks contained in Ω.*

A key difference of Definition 2 between $\mathcal{M}$ and $\mathbb{R}^2$ follows. If a point $s \in S(\Omega)$ has at least two different closest points in $\mathcal{M} \setminus \Omega$, s is called a medial axis point. In $\mathbb{R}^2$, medial axis points are dense in $S(\Omega)$; while in $\mathcal{M}$, $S(\Omega)$ may have no medial axis points at all. One example is illustrated in Figure 3.

In most cases, $S(\Omega)$ is a closed set. However, it was shown in [24] that $S(\Omega)$ is not necessarily a closed set and an example of $S(\Omega)$ being an open set was given in $\mathbb{R}^2$. Thus, following [24], we study the mapping $\Omega \to \overline{S}(\Omega)$ from $\mathcal{O}$ to $\mathcal{C}$, where $\overline{S}(\Omega)$ is the closure of $S(\Omega)$.

Distinct from its Euclidean counterpart in $\mathbb{R}^2$, $S(\Omega)$ in $\mathcal{M}$ has some specific properties. Below we show that a connected open region $\Omega \subset \mathcal{M}$ may have a disconnected skeleton $\overline{S}(\Omega)$. As a comparison, Matheron [24] proved that in $\mathbb{R}^2$, if Ω is connected, $\overline{S}(\Omega)$ is also connected.

First we show that the bisector of two points in $\mathcal{M}$ is not necessarily a curve but may contain 2D regions. Let p and q be two points in $\mathbb{R}^2$. r lies on the bisector of p and q with angle $\angle prq = \alpha$. Then we cut a region in $\mathbb{R}^2$ and plug in a folded triangle fan with a spanning angle $\gamma > 2\alpha$ (the shaded region shown in Figure 4) to form a 2-manifold $\mathcal{M}_T$. The geodesic distance in the area of the folded triangle fan in $\mathcal{M}_T$ is determined by unfolding the triangle fan along the boundary lines $\overline{pr}$ and $\overline{qr}$, respectively [25]. Then, as shown in Figure 4, inside the folded triangle fan, the yellow (or blue) region has a shorter geodesic distance to point p (or q), and the uncolored area with spanning angle $\gamma - 2\alpha$ lies on the bisector of p and q in $\mathcal{M}_T$.

Next we show that the skeleton of a connected region in $\mathcal{M}$ and its closure are not necessarily connected. Let the shaded region in Figure 5 be the 2D bisector with a spanning angle $\gamma - 2\alpha$ as identified in Figure 4. Note that the shaded region is a folded polygonal region which does not lie in the same plane spanned by points p, q and r. In the shaded region, if points x_1, x_2 and r are not in the same line, then x_1 and x_2 satisfy the triangle inequality $|d_g(x_1, r) - d_g(x_2, r)| < d_g(x_1, x_2)$. By Property 1, $D_{d_g(x_1,p)}(x_1) \not\subset D_{d_g(x_2,p)}(x_2)$ and $D_{d_g(x_2,p)}(x_2) \not\subset D_{d_g(x_1,p)}(x_1)$[4]. Then along any direction in the spanning angle $\gamma - 2\alpha$ (middle left in Figure 5), there is a maximal disk whose boundary touches points p and q. Let Arc be a circular arc in the shaded region which has equal distance to r, and LS be a line segment which is the bisector

3. In $\mathbb{R}^2$ a connected closed set may have a disconnected skeleton; see the example at page 219 in [24].

4. Note that $d_g(x_1, r) + d_g(r, p) = d_g(x_1, p)$ and $d_g(x_2, r) + d_g(r, p) = d_g(x_2, p)$.

part of p and q in the planar region (middle right in Figure 5). Note that one endpoint of LS is open (hollow circle in Figure 5). It is readily seen that $\Omega = \bigcup_{x \in Arc \bigcup LS} D_{d_g(x,p)}(x)$ is a connected open set in $\mathcal{M}_T$ and $S(\Omega) = Arc \bigcup LS$. $S(\Omega)$ is not closed due to the open end in LS and $\overline{S}(\Omega)$ consists of two disjoint subsets Arc and $\overline{LS}$. As a comparison, the skeleton of $\mathbb{R}^2 \setminus \{p, q\}$ is the bisector of p and q (far right in Figure 5), since any two points x_1 and x_2 in the bisector satisfying $d_g(x_1, x_2) > |d_g(p, x_1) - d_g(p, x_2)|$. We have:

Property 3. *For a connected open set $\Omega \in \mathcal{M}$, the skeleton $S(\Omega)$ is not necessarily closed and $\overline{S}(\Omega)$ is not necessarily connected.*

5 Semi-Continuity of Mapping $\Omega \to \overline{S}(\Omega)$

Recall that $\mathcal{O}$ and $\mathcal{C}$ are the collections of all the open sets and closed sets in $\mathcal{M}$ respectively. For an open set $\Omega \in \mathcal{O}$, the mapping $\Omega \to \overline{S}(\Omega)$ from $\mathcal{O}$ to $\mathcal{C}$ maps Ω to the closure of the skeleton $S(\Omega)$. We consider a sequence $\{\Omega_i\}$ that converge to Ω in $\mathcal{O}$, i.e., $\lim\{\Omega_i\} = \Omega$. There is a corresponding sequence $\{\overline{S}(\Omega_i)\}$ and in this section we study the convergence of $\{\overline{S}(\Omega_i)\}$ in $\mathcal{C}$.

Let $\{c_i\}$ be a sequence in $\mathcal{C}$. Denote by $\underline{\lim}\{c_i\}$ (resp. $\overline{\lim}\{c_i\}$) the intersection (resp. union) of the accumulation points of $\{c_i\}$ in $\mathcal{M}$. Let $\{o_i\}$ be a sequence in $\mathcal{O}$ that converge to o.

Definition 3. *[28] For a mapping F from $\mathcal{O}$ to $\mathcal{C}$,*

- *F is upper semi-continuous if and only if $F(o) \supset \overline{\lim}\{F(o_i)\}$. i.e., if a closed set A is disjoint from $F(o)$, there exists a N_A such that A is disjoint from all the $F(o_i)$, $\forall i > N_A$.*
- *F is lower semi-continuous if and only if $F(o) \subset \underline{\lim}\{F(o_i)\}$. i.e., if an open set B intersects $F(o)$, there exists a N_B such that B intersects all the $F(o_i)$, $\forall i > N_B$.*

Property 4. *The mapping $\Omega \to \overline{S}(\Omega)$ from $\mathcal{O}$ to $\mathcal{C}$ is lower semi-continuous.*

We prove Property 4 in two steps.

- Step 1. For each maximal disk $MD \subset \Omega$, we prove that there exists a sequence $\{MD_i\}$ of maximal disks, which converge to MD in $\mathcal{O}$, where $MD_i \subset \Omega_i$ and $\lim\{\Omega_i\} = \Omega$.
- Step 2. Prove Property 4 using the result of Step 1.

A similar result was presented in [24] for skeletons of open sets in $\mathbb{R}^2$. Our study extends their result from $\mathbb{R}^2$ to $\mathcal{M}$, with a more general proof.

5.1 Proof of Step 1

For a maximal disk $MD \subset \Omega$, let $\mathcal{O}_{MD}$ be the collection of all the open sets in $\mathcal{M}$ that intersect MD, i.e., $\forall o_i \in \mathcal{O}_{MD}$, $o_i \cap MD \neq \emptyset$. Let $\mathcal{C}_{MD}$ be the collection of all the closed sets in $\mathcal{M}$ that are disjoint from MD, i.e., $\forall c_i \in \mathcal{C}_{MD}$, $c_i \cap MD = \emptyset$. By Definition 1, to prove Step 1, we need to show that (1) $\forall o \in \mathcal{O}_{MD}$, there exists an N_O such that $\forall i > N_O$, o intersects all the MD_i (Proposition 1), and (2) $\forall c \in \mathcal{C}_{MD}$, there exists an N_C such that $\forall j > N_C$, c is disjoint from all the MD_j (Proposition 2).

Proposition 1. *$\forall o \in \mathcal{O}_{MD}$, there exists an N_O and a maximal disk sequence $\{MD_i\}$ such that $\forall i > N_O$, MD_i intersects o, where $MD_i \subset \Omega_i$ and $\lim\{\Omega_i\} = \Omega$.*

Proof. Let p be the center of MD with a radius r_{MD}, i.e., $MD = D_{r_{MD}}(p) = \{q \in \mathcal{M} | d_g(p, q) < r_{MD}\}$. Let $\{r_i\}$ be a sequence of positive scalar values, which monotonic-sequentially converge to r_{MD}, i.e., $r_i \uparrow r_{MD}$, $r_i < r_{i+1} < r_{MD}$. Correspondingly there is a sequence $\{D_i\}_{i \in J}$ with an index set J, $D_i = D_{r_i}(c)$, of concentric disks in Ω such that $\forall i \in J$, $D_i \subset D_{i+1}$, and $\lim\{D_i\} = MD$. Then there exists an N_1 such that $\forall i > N_1$, D_i intersects o.

Next we show that there exists an N_2 such that $\forall i > N_2$, $D_i \subset \Omega_i$. If it is not true, then there exists an open set $o' \in \mathcal{O}$ that intersects all the D_i, but does not intersect all the Ω_i, $\forall i > N_2$ (note that $D_i \subset D_{i+1}$). Since $D_i \subset MD$, $MD \subset \Omega$, o' must intersect MD and Ω. On the other hand, since o' does not intersect all the Ω_i, $\forall i > N' > N_2$, and $\{\Omega_i\}$ converge to Ω, o' cannot intersect Ω. A contradiction.

By Property 2, $\forall i > N_2$, each D_i is contained in a maximal disk $MD_i \subset \Omega_i$. Let $N_O = \max\{N_1, N_2\}$. That completes the proof. □

Proposition 2. *For the same sequence $\{MD_i\}$ as in Proposition 1, $\forall c \in \mathcal{C}_{MD}$, there exists a $N_C > N_O$ such that $\forall i > N_C$, MD_i is disjoint from c.*

Proof. We prove this proposition by contradiction. Suppose for any sufficiently large N'', $\exists i > N''$, MD_i intersects some $c \in \mathcal{C}_{MD}$. Then there exists at least a point $x \in c$ which satisfies $x \in MD_i$ and $x \notin MD$. Since $D_i \subset MD_i$, there is a contradiction in that $\{D_i\}$ converge to MD and MD is a maximal disk in Ω. □

5.2 Proof of Step 2

In the proof of Step 1, we show that for any maximal disk $MD \subset \Omega$, there exists a sequence $\{MD_i\}$ of maximal disks, $MD_i \subset \Omega_i$, that converge to MD. Let the centers of MD and MD_i be p and p_i, respectively. For each point $p \in \overline{S}(\Omega)$, there exists a sequence $\{p_i\}$ of points that converge to p, such that $\forall i$, $p_i \subset S(\Omega_i)$. Accordingly, if an open set B intersects $\overline{S}(\Omega)$, there exists a N_B such that B intersects all the $\overline{S}(\Omega_i)$, $\forall i > N_B$. Thus the mapping $\Omega \to \overline{S}(\Omega)$ is lower semi-continuous.

5.3 Manifold with Boundary

The above proof of Property 4 requires that $\mathcal{M}$ is a connected, closed 2-manifold. Let $\mathcal{M}'$ is a connected, compact 2-manifold with boundary. In this section we show that Property 4 also holds for $\mathcal{M}'$.

Denote the boundary of $\mathcal{M}'$ by $\partial\mathcal{M}'$. First, note that an open set Ω in $\mathcal{M}'$ cannot contain a point in $\partial\mathcal{M}'$, i.e., $\Omega \cap \partial\mathcal{M}' = \emptyset$. Let $G = \{g_1, g_2, \cdots, g_n\}$, $n \geq 1$, be the set of connected components in $\partial\mathcal{M}'$. Each $g_i \in G$ is a closed curve and we can always glue a cap m_i (i.e., another 2-manifold with the same boundary g_i) to remove g_i from G. Then $\overline{\mathcal{M}} = \mathcal{M}' \cup (\cup_{i=1}^{n} m_i)$ is a connected, closed 2-manifold.

By Property 4, the mapping $\Omega \to \overline{S}(\Omega)$ is lower semi-continuous in $\overline{\mathcal{M}}$. Since $\Omega \cap \partial\mathcal{M}' = \emptyset$, for any sequence $\{\Omega_i\}$ that converge to Ω in $\overline{\mathcal{M}}$, there exists an N such that $\forall i > N$, $\Omega_i \cap \partial\mathcal{M}' = \emptyset$ and $\Omega_i \subset \mathcal{M}'$. Therefore the mapping $\Omega \to \overline{S}(\Omega)$ is also lower semi-continuous in $\mathcal{M}'$.

6 Skeleton Approximation

The result in Property 4 is useful in pattern analysis and computer vision. Below we list some applications, in each of which a shape sequence $\{\Omega_i\}$ converge to a shape Ω. Then by Property 4, the limit of $\{\overline{S}(\Omega_i)\}$ contains $\overline{S}(\Omega)$.

- Curve evolution. Based on a psychophysically relevant representation of visual parts, a novel decomposition rule was proposed in [17] for shape contour evolution. The shape is defined in $\mathbb{R}^2$ and can be extended to a 2-manifold $\mathcal{M}$. The process of shape evolution forms a sequence of shapes from the coarse level to fine detail level that converge to the original shape.
- Morphology on 2-manifolds. For a shape $\Omega \in \mathcal{M}$, we define the dilation as $\Omega \oplus D_\rho = \bigcup_{p\in\Omega} D_\rho(p)$ and the erosion as $\Omega \ominus D_\rho = \{p \in \mathcal{M} | D_\rho(p) \subset \Omega\}$. Then given a sequence $\{\rho_i\}$ of disk radii which converge to $\rho = 0$, the dilation $\Omega \oplus D_\rho$ or erosion $\Omega \ominus D_\rho$ gives a sequence $\{\Omega_i\}$ that converge to Ω.
- Point approximation. Let $\partial\Omega$ be the boundary of a shape $\Omega \subset \mathcal{M}$. If we sample $\partial\Omega$ using points and make the samples denser and denser, the sequence of point sets converge to $\partial\Omega$.

In these applications, if the skeleton $\overline{S}(\Omega_i)$ in the shape sequence $\{\Omega_i\}$ can be computed much easier than $\overline{S}(\Omega)$, we can use $\overline{S}(\Omega_i)$ as an approximation of $\overline{S}(\Omega)$. In this section we show that this approximation is good in the sense that the skeletons of Ω_i contain the skeleton of a small perturbation of Ω.

6.1 Voronoi Skeleton of Point Sampling

Let Ω be a connected open set in $\mathcal{M}$. Note that $\Omega^- = \mathcal{M} \setminus \partial\Omega$ is also open. If $P = \{p_1, p_2, \cdots, p_m\}$, $p_i \neq p_j$, is a set of sample points of $\partial\Omega$, $\overline{S}(\mathcal{M} \setminus P)$ is an approximation of $\overline{S}(\Omega^-)$ and $\overline{S}(\mathcal{M} \setminus P) \bigcap \Omega$ is an approximation of $\overline{S}(\Omega)$.

The Voronoi cell of $p_i \in P$ in $\mathcal{M}$ is defined as

$$VC(p_i) = \{q | d_g(q, p_i) \leq d_g(q, p_j), i \neq j, q \in \mathcal{M}\}$$

A boundary-based Voronoi diagram of P is defined as

$$VD(P) = \bigcup_i \partial VC(p_i)$$

where $\partial VC(p_i)$ is the boundary of $VC(p_i)$. For each point $p_i \in P$, we denote by $PB(p_i) \subset VC(p_i)$ the set of points which satisfy $\forall x \in PB(p_i)$, the boundary of a maximal disk centering at x touches p_i at least twice (Figure 3). $PB(p_i)$ is actually the cut loci of p_i [37] and is called the pseudo-bisector in [20]. We define an extended boundary-based Voronoi diagram of P as

$$EVD(P) = VD(P) \bigcup \left(\bigcup_i PB(p_i) \right)$$

Property 5. $S(\mathcal{M} \setminus P) \subset EVD(P)$.

Proof. $\Omega' = \mathcal{M} \setminus P$ is an open set in $\mathcal{O}$. By Definition 2, $S(\Omega')$ is a set of centers of maximal disks in Ω'. Note that the interior of any maximal disk contains none of the points in P. There are two cases of maximal disks in Ω'. The first case is the boundary of a maximal disk touches at least two different points in P. In this case, the centers of maximal disks are in $VD(P)$. The second case is the boundary of a maximal disk touches one point in P twice (Figure 3). In this case, the centers of maximal disks are in $\bigcup_i PB(p_i)$. That completes the proof. □

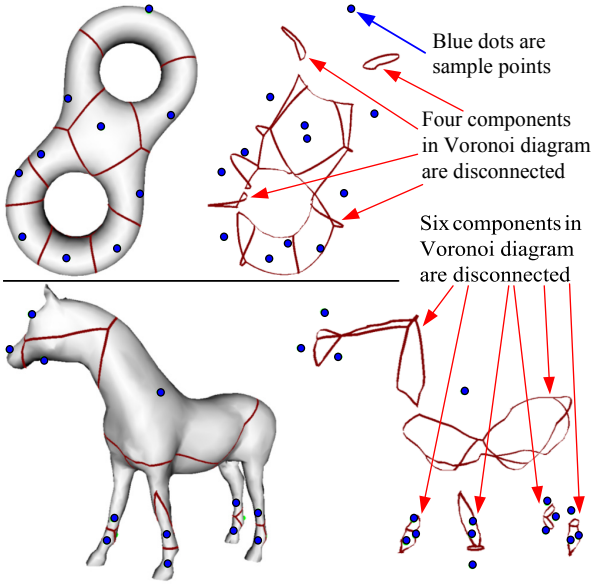

Fig. 6. Disconnected boundary-based Voronoi diagrams in $\mathcal{M}$. Some sample points are at the back of the model (right) and cannot be viewed when the surface is shaded (left). Top: 2-manifold of genus 2. Bottom: 2-manifold of genus 0.

Note that $S(\mathcal{M} \setminus P)$ may not be equal to $EVD(P)$. For example, the shaded region in Figure 5 is the 2D bisector of points p and q, but only the Arc is in the skeleton. By Property 3, $\overline{S}(\Omega)$ may be disconnected. Note that the boundary-based Voronoi diagram $VD(P)$ of a sampling P may be also disconnected; two examples are shown in Figure 6.

Let $VS(P) = EVD(P) \bigcap \Omega$. If P is a dense sampling of $\partial\Omega$, we use $EVD(P)$ and $VS(P)$ as approximations of $S(\mathcal{M} \setminus \partial\Omega)$ and $S(\Omega)$ respectively. We call $VS(P)$ the Voronoi skeleton of Ω under the sampling P.

6.2 A Hierarchy of Voronoi Skeletons

Let P be a sampling of $\partial\Omega$. If there are g holes inside Ω, $\partial\Omega$ consists of $g+1$ disjoint closed curves and let $P = \{(p_{11}, \cdots, p_{1m_1}), \cdots, (p_{i1}, \cdots, p_{im_i}), \cdots, (p_{(g+1)1}, \cdots, p_{(g+1)m_{g+1}})\}$. We define an ordering in P as follows: (1) the sampling in each closed curve is periodic, i.e., $\forall i$, $p_{i(m_i+1)} = p_{i1}$; (2) when one walks along the boundary from p_{ij} to $p_{i(j+1)}$, $\forall i, j$, Ω is always on the left-hand side. Whenever there is no risk of confusion, we use the concise form $P = \{p_1, p_2, \cdots, p_m\}$ and set the number of sample points $m \geq 3$.

We use the r-regular model in [28] to study a sampling criterion of P:

Definition 4. *The shape Ω is called r-regular, if $\Omega = (\Omega \ominus D_r) \oplus D_r = (\Omega \oplus D_r) \ominus D_r$, where $\Omega \oplus D_\rho = \bigcup_{p\in\Omega} D_\rho(p)$ and $\Omega \ominus D_\rho = \{p \in \mathcal{M} | D_\rho(p) \subset \Omega\}$.*

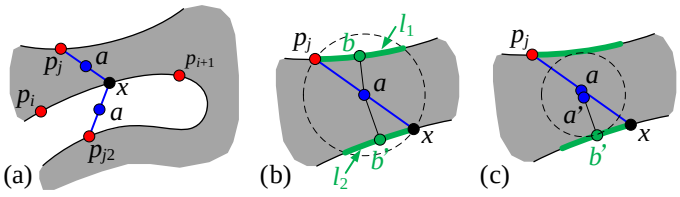

Fig. 7. Proof of Property 6. The shaded area is Ω and the blank area is $\mathcal{M} \setminus \Omega$. (a) If the closest sample point to x is p_j (or p_{j2}), the midpoint a of the shortest path $\overline{xp_j}$ (or $\overline{xp_{j2}}$) is inside Ω (or $\mathcal{M} \setminus \Omega$). (b) Disk $D_{r_a}(a)$ of radius $r_a = d_g(a,x) < r$ contains two connected components of $\partial\Omega$, i.e., l_1 and l_2 (green colored curves). b is the closest point of a on $\partial\Omega$, $b \in l_1$, and b' is the closest point of a on l_2. (c) a' is a point in the path $\overline{ab'}$ which has equal distance to l_1 and l_2. $D_{r_{a'}}(a')$ is a maximal disk in Ω whose radius $r_{a'} = d_g(a',b') < r$.

Definition 5. *P is called an ε-sampling of $\partial\Omega$, if $\forall x \in \partial\Omega$, $\min\{d_g(x,p_i)|p_i \in P\} \leq \varepsilon$.*

Denote by $B(p_i,p_j) \subset \mathcal{M}$ the bisector between p_i and p_j. Let $C_{i(i+1)}$ be the segment in $\partial\Omega$ that has two endpoints p_i and p_{i+1} and does not pass through any other points in P.

Property 6. *For an ε-sampling P of an r-regular shape Ω in $\mathcal{M}$, if $\varepsilon < 2r$, then $\forall x \in C_{i(i+1)}$, the closest sample point in P is either p_i or p_{i+1}.*

Proof. Note that if Ω is an r-regular shape, all the maximal disks in Ω and $\mathcal{M} \setminus \Omega$ have radii no smaller than r. Below we show that if Property 6 is not true, then there exists a maximal disk in either Ω or $\mathcal{M} \setminus \Omega$ such that its radius is smaller than r.

Refer to Figure 7(a). If Property 6 is not true, then there exists a point $x \in C_{i(i+1)}$ such that the closest sample point to x is p_j, $j \neq i$, $j \neq i+1$. Since P is ε-sampling, $d_g(x,p_j) \leq \varepsilon$. Denote by $\overline{xp_j}$ the shortest path between x and p_j in $\mathcal{M}$. Let a be the midpoint of $\overline{xp_j}$, i.e., $a \in \overline{xp_j}$ and $d_g(a,x) = d_g(a,p_j) < r$. Below we show that if $a \in \Omega$, then in Ω there exists a maximal disk whose radius is smaller than r. If $a \notin \Omega$, a similar argument can show that in $\mathcal{M} \setminus \Omega$ there exists a maximal disk whose radius is smaller than r.

Assume $a \in \Omega$. If the disk $D_{r_a}(a)$ of radius $r_a = d_g(a,x) < r$ is a maximal disk in Ω, then we are done. Otherwise, the disk $D_{r_a}(a)$ contains two connected components of $\partial\Omega$, since $D_{r_a}(a)$ cannot contain any sample point $p_k \in P$ in its interior. Refer to Figure 7(b). Denote these two connected components by l_1 and l_2. Denote by b the closest point of a on $\partial\Omega$. Without loss of generality, assume $b \in l_1$. Let b' be the closest point of a on l_2. If $d_g(a,b) = d_g(a,b')$, then $D_{r'=d_g(a,b)}(a)$ is a maximal disk in Ω whose radius $r' = d_g(a,b) < r$. Otherwise, for any point in the shortest path $\overline{ab'}$, its closest point on $\partial\Omega$ must be on l_1 or l_2. Refer to Figure 7(c). Now moving a to b' along the path $\overline{ab'}$. During this movement, the closest point of a is changed from l_1 to l_2 and there must exist a critical point a' in $\overline{ab'}$ such that it has two closest points on $\partial\Omega$: one is in l_1 and the other is $b' \in l_2$. Then $D_{r_{a'}}(a')$ is a maximal disk in Ω whose radius $r_{a'} = d_g(a',b') < r$. □

Note that the proof of Property 6 is similar to the ones in [2], [3], [5] in which, however, a different result of a ball containing at least one skeleton point is obtained.

Property 7. *For an ε-sampling P of an r-regular shape Ω in $\mathcal{M}$, if $\varepsilon < 2r$, then $VC(p_i) \bigcap \partial\Omega = VC(p_i) \bigcap (C_{(i-1)i} \bigcup C_{i(i+1)})$.*

Proof. Suppose in addition to $C_{(i-1)i} \bigcup C_{i(i+1)}$, there is another portion C' of $\partial\Omega$ inside $VC(p_i)$. Since C' is disjoint from $VC(p_i) \bigcap (C_{(i-1)i} \bigcup C_{i(i+1)})$, when walking around $\partial\Omega$ in a counterclockwise order, p_{i+1} must be in-between $VC(p_i) \bigcap (C_{(i-1)i} \bigcup C_{i(i+1)})$ and C', and p_{i-1} must be in-between C' and $VC(p_i) \bigcap (C_{(i-1)i} \bigcup C_{i(i+1)})$. Then by Property 6, the closest sample point to $x \in C'$ is p_j, $j \neq i$; however $x \in VC(p_i)$, a contradiction. □

Based on Property 7, the Voronoi diagram $VD(P)$ of an ε-sampling P is well structured since we can reconstruct a piecewise linear approximation $\partial\Omega'$ of $\partial\Omega$ from P such that the approximation error $Error(\partial\Omega', \partial\Omega) = \sup_{x \in \partial\Omega} \inf_{y \in \partial\Omega'} d_g(x,y) \leq \varepsilon$. Some similar results that reconstruct a curve from dense sample points in a Euclidean plane $\mathbb{R}^2$ had been studied (e.g., [10]). Our result extends them from $\mathbb{R}^2$ to a 2-manifold $\mathcal{M}$.

Since for $\lim\{P_i\} = \partial\Omega$, $S(\Omega) \subset \underline{\lim}\{VS(P_i)\}$ and some subsets in $VS(P)$ may be redundant (e.g., the bisector $B(p_i,p_{i+1})$ locally around $\partial\Omega$ is usually redundant), we present a hierarchy of Voronoi skeletons which give a level-of-detail approximation of $S(\Omega)$.

Definition 6. *For any bisector $B(p_i,p_j) \subset VD(P)$, the granularity of $B(p_i,p_j)$ is defined as $g(B(p_i,p_j)) = |j-i|$.*

Definition 7. *The boundary-based Voronoi diagram of P at granularity k is defined as $VD(P)|_k = \{B(p_i,p_j)|B(p_i,p_j) \subset VD(P), |j-i| \geq k\}$. The Voronoi skeleton at granularity k is $VS(P)|_k = (VD(P)|_k \bigcup (\bigcup_i PB(p_i))) \bigcap \Omega$.*

For an ε-sampling $P = \{p_1, p_2, \cdots, p_m\}$ of an $r(> \varepsilon/2)$-regular shape $\Omega \subset \mathcal{M}$, the Voronoi skeletons $VS(P)|_k$ from granularity $k = \lceil m/2 \rceil - 1$ to 1 give a hierarchy of approximations to $S(\Omega)$. One example of $VS(P)|_k$ at $k = 20$ and 3 is illustrated in Figure 1.

$\forall x \in S(\Omega)$, let $r_{MD}(x)$ be the radius of the maximal disk in Ω centered at x and $S_\lambda(\Omega) = \{x \in S(\Omega) | r_{MD}(x) \geq \lambda\}$. Inspired by a novel λ-medial axis in $\mathbb{R}^n$ [9], below we show that the Voronoi skeleton $VS(P)$ is a good approximation since it contains the skeleton of a small perturbation of Ω:

Property 8. *For an ε-sampling P of $\partial\Omega$, if $\lambda > \varepsilon$, then $S_\lambda(\Omega') \subset VS(P)$, where $\Omega' = (\Omega \oplus D_\varepsilon) \setminus P$.*

Proof. We prove this property by showing that for all maximal disks MD in Ω', $\partial MD \cap \partial(\Omega \oplus D_\varepsilon) = \emptyset$. If it is not true, let $MD_r(x)$, $x \in S(\Omega')$ and $r > \varepsilon$, be such a maximal disk whose boundary contains a point $z \in \partial(\Omega \oplus D_\varepsilon)$. Then in a geodesic path from z to x in Ω' there exists a point $y \in \partial\Omega$. By Property 1, $D_\varepsilon(y) \subset MD_r(x)$. Since P is an ε-sampling of $\partial\Omega$, $\overline{D_\varepsilon(y)}$ as well as $MD_r(x)$ contain at least a point in P; a contradiction to the fact that $MD_r(x)$ is inside Ω'. □

6.3 Applications

If Ω is bounded by piecewise smooth curves in a smooth 2-manifold $\mathcal{M}$, it is generally difficult to compute $S(\Omega)$ exactly. One practical way to compute an approximation of $S(\Omega)$ is to approximate $\mathcal{M}$ by a 2-manifold triangular mesh $\mathcal{T}$ and use numerical solutions of Hamilton-Jacobi equations on $\mathcal{T}$ [27], [30], [31]. However, these numerical

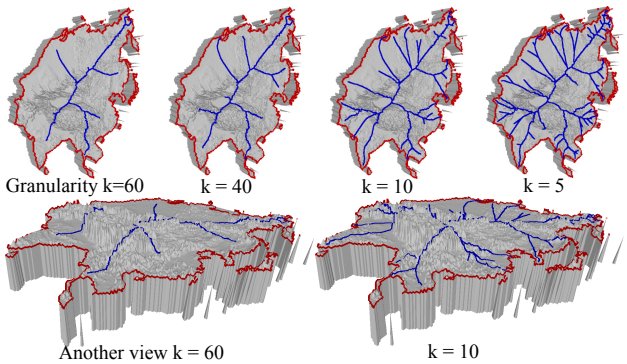

(a) Voronoi skeletons of one connected component in the topographical surface of Asia

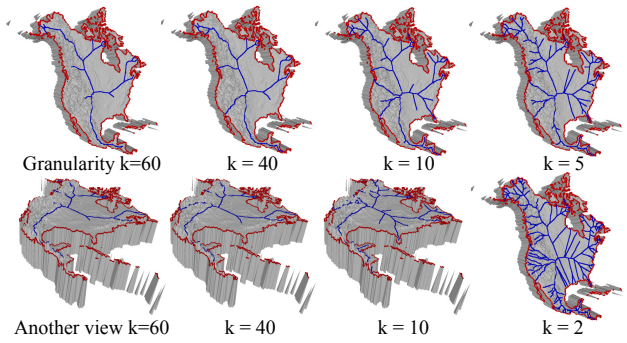

(b) Voronoi skeletons of one connected component in the topographical surface of North America

Fig. 8. Voronoi skeletons in topographical surfaces of Asia and North America at different granularities. Full illustrations of Voronoi skeletons of five continents, including Africa, Asia, Europe, North America and South America, are presented in supplemental material A.

Model name	Tri. No	Boundary Sample Pt.	Time (sec.)
Africa	88,163	596	5.878
Asia	63,684	981	7.614
Europe	50,464	754	3.309
North America	60,788	1,158	4.211
South America	45,748	522	4.759

TABLE 1
The statistical data of computing Voronoi skeletons in topographical surfaces in Fig. 8 and supplemental material A. The running time is measured using a PC with Intel(R) i7-2600 CPU running at 3.4GHz.

solutions may suffer from the triangular shape and triangle distribution in $\mathcal{T}$; e.g., the numerical error may be much smaller in congruent triangles of equal sizes than that in sliver triangles of non-uniform sizes. In this study, we use the computational geometry method [20], [21] based on an exact geodesic [19] to compute the Voronoi skeleton as a good approximation to $S(\Omega)$. Compared to the numerical solutions to PDEs, the computational geometry method is accurate and not sensitive to the triangular shape and triangles' distribution in $\mathcal{T}$.

Let V be the mesh vertex set in $\mathcal{T}$. $\mathcal{T}$ is said to be *non-degenerated* if $\forall v_k \in V$, $\forall p_i, p_j \in P$, $i \neq j$, $d_g(v_k, p_i) \neq d_g(v_k, p_j)$. It was shown in [20] that if $\mathcal{T}$ is non-degenerated, 2D bisectors can not appear in $VD(P)$ and $VD(P)$ is a collection of finite 1D curve segments. If a mesh $\mathcal{T}'$ is degenerated, we can slightly disturb the positions of those violated vertices such that the resulting mesh $\mathcal{T}$ is non-degenerated. In all the examples presented in this section, we preprocess each mesh surface $\mathcal{T}$ such that $\mathcal{T}$ is non-degenerated.

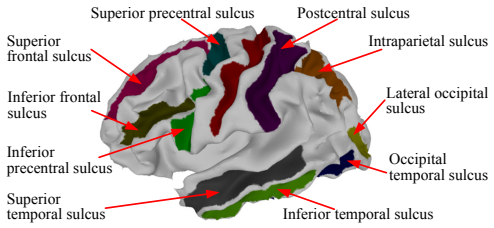

Fig. 9. Parts of sulcal shapes in the cortical surface of human brain.

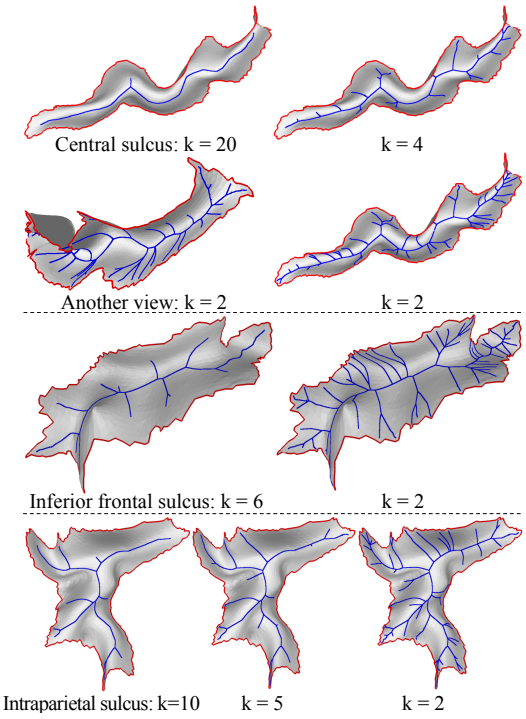

Fig. 10. Voronoi skeletons of three sulci at different granularities. Full illustration of Voronoi skeletons of 14 major sulci are presented in supplemental material B.

Skeletons can find a wide range of applications in pattern analysis [33], from the large scale such as the stellar arrangement in galaxies to the small scale such as the pattern representation of molecular structures. Below we present two applications in topography and brain morphometry.

In topography, skeletons in a topographical surface can be used to estimate a drainage network from basin boundaries, or estimate the lengths of mountain chains, canyons, rivers, roads and other elongated structures. A method that uses the medial axis in a topographical mesh was proposed in [11] for designing continuous cartograms. Figure 8 shows topographical surfaces of two continents, Asia and North America. The boundary of one connected component in each topographical surface is sampled by points (the number of sample points is summarized in Table 1). A Voronoi skeleton for each boundary is computed only once and can be illustrated at different granularities (Figure 8). The Voronoi skeletons of five continents are illustrated in supplemental material A. The data in Table 1 demonstrates that the computation of Voronoi skeletons is fast; i.e., less than ten seconds for 2-manifold meshes of nearly 100k triangles.

In brain morphometry, recent advances have attracted

considerable attention for constructing a graphical representation of cortical folding patterns [35]. Skeleton-based methods on the cortical surface became popular due to the representation of intrinsic geometry [31]. The cortical surface can be segmented into labeled gyri by a set of sulci (Figure 9). We sample the boundaries of sulcal regions by points and build the Voronoi skeletons. Figure 10 illustrates Voronoi skeletons of three sulci at different granularities. The Voronoi skeletons of 14 major sulci are illustrated in supplemental material B. All sulcal shapes have hundreds of triangles and the computation of all sulcal Voronoi skeletons are less than one second.

7 Conclusion

In this paper we study the skeleton in a 2-manifold $\mathcal{M}$ and show several properties that distinguish it from its Euclidean counterpart in $\mathbb{R}^2$; i.e., the closure $\overline{S}(\Omega)$ of skeleton is not necessarily connected for a connected region $\Omega \subset \mathcal{M}$ and a skeleton in $\mathcal{M}$ may have no medial axis points at all. We prove that when a sequence $\{\Omega_i\}$ converge to a shape $\Omega \subset \mathcal{M}$, the mapping $\Omega \to \overline{S}(\Omega)$ is lower semi-continuous. Finally some applications of these results on sample-point-based Voronoi skeleton approximations are presented.

Acknowledgements

The author thanks the editor and reviewers very much for their constructive comments that help improve this paper. The topographical data (Figure 8) and sulci data (Figure 10) are courtesy of U.S. Geological Survey and Computational Functional Anatomy Lab at National University of Singapore. This work was supported by the Natural Science Foundation of China (61322206, 61432003, 61272228) and the National Basic Research Program of China (2011CB302202).

References

[1] A.D. Aleksandrov and V.A. Zalgaller, *Intrinsic Geometry of Surfaces*, AMS Publisher, 1967.
[2] N. Amenta and M. Bern, "Surface Reconstruction by Voronoi Filtering," Discrete & Computational Geometry , vol.22, no.4, pp. 481-504, 1999.
[3] D. Attali, H. Edelsbrunner and Y. Mileyko, "Weak Witnesses for Delaunay Triangulations of Submanifolds," In Proc. ACM Symposium on Solid and Physical Modeling, pp. 143-150, 2007.
[4] H. Blum and R.N. Nagel, "Shape Description Using Weighted Symmetric Axis Features," Pattern Recognition, vol.10, no.3, pp. 167-180, 1978.
[5] J.D. Boissonnat and F. Cazals, "Natural Neighbor Coordinates of Points on a Surface," Computational Geometry: Theory and Applications, vol.19, no.2-3, pp. 155-173, 2001.
[6] M.P. do Carmo, *Differential Geometry of Curves and Surfaces*, Pearson Education, Inc., 1976.
[7] F. Chazal and R. Soufflet, "Stability and Homotopy of a Subset of the Medial Axis," In Proc. 9th ACM Symp. Solid modeling Appl., pp. 243-248, 2004.
[8] F. Chazal and R. Soufflet, "Stability and Finiteness Properties of Medial Axis and Skeleton," Journal of Dynamical and Control Systems, vol.10, no.2, pp. 149-170, 2004.
[9] F. Chazal and A. Lieutier, "The λ-Medial Axis," Graphical Models, vol.67, no.4, pp. 304-331, 2005.
[10] T.K. Dey, K. Mehlhorn and E.A. Ramos, "Curve Reconstruction: Connecting Dots with Good Reason," Computational Geometry, vol.15, no.4, pp. 229-244, 2000.
[11] D.A. Keim, A.C. Panse and S.C. North, "Medial-Axis-Based Cartograms," IEEE Computer Graphics and Applications, vol.25, no.3, pp. 60-68, 2005.
[12] B.B. Kimia, A. Tannenbaum and S. Zucker, "Shape, Shocks and Deformation I: The Components of Two-Dimensional Shape and The Reaction-Diffusion Space," International Journal of Computer Vision, vol.15, no.3, pp. 189-224, 1995.
[13] R. Kimmel, N. Kiryati and A. Bruckstein, "Multivalued Distance Maps for Motion Planning on Surfaces with Moving Obstacles," IEEE Trans. Robotics and Automation, vol.14, no.3, pp. 427-436, 1998.
[14] R. Kimmel, R. Malladi and N. Sochen, "Images as Embedded Maps and Minimal Surfaces: Movies, Color, Texture, and Volumetric Medical Images," International Journal of Computer Vision, vol.39, no.2, pp. 111-129, 2000.
[15] R. Kimmel and J.A. Sethian, "Computing Geodesic Paths on Manifolds," Proc. of National Academy of Science, vol.95, no.15, pp. 8431-8435, 1998.
[16] R. Lai, *Computational Differential Geometry and Intrinsic Surface Processing*, PhD thesis, Department of Mathematics, University of California, Los Angeles, 2010.
[17] L.J. Latecki and R. Lakamper, "Convexity Rule for Shape Decomposition Based on Discrete Contour Evolution," Computer Vision and Image Understanding, vol.73, no.3, pp. 441-454, 1999.
[18] A. Lieutier, "Any open bounded subset of R^n has the same homotopy type as its medial axis," Computer-Aided Design, vol.36, no.11, pp. 1029–1046, 2004.
[19] Y.J. Liu, "Exact Geodesic Metric in 2-Manifold Triangle Meshes Using Edge-based Data Structures," Computer-Aided Design, vol.45, no.3, pp. 695-704, 2013.
[20] Y.J. Liu, Z. Chen and K. Tang, "Construction of Iso-contours, Bisectors and Voronoi Diagrams on Triangulated Surfaces," IEEE Trans. Pattern Analysis and Machine Intelligence, vol.33, no.8, pp. 1502-1517, 2011.
[21] Y.J. Liu and K. Tang, "The Complexity of Geodesic Voronoi Diagrams on Triangulated 2-Manifold Surfaces," Information Processing Letters, vol.113, no.4, pp. 132-136, 2013.
[22] T. Maekawa, "Computation of Shortest Paths on Free-Form Parametric Surfaces," Journal of Mechanical Design, vol.118, no.4, pp. 499-508, 1996.
[23] G. Matheron, *Random Sets and Integral Geometry*, J. Wiley and Sons: New York, 1975.
[24] G. Matheron, "Examples of Topological Properties of Skeletons," in Image Analysis and Mathematical Morphology, Volume 2: Theoretic Advances, J. Serra ed., pp. 217-238, 1988.
[25] J. Mitchell, D.M. Mount, and C.H. Papadimitriou, "The Discrete Geodesic Problem," SIAM Journal of Computing, vol. 16, no. 4, pp. 647-668, 1987.
[26] J.R. Munkres, *Topology*, second ed., Prentice Hall, 2000.
[27] S.J. Osher and R.P. Fedkiw, *Level Set Methods and Dynamic Implicit Surfaces*, Springer-Verlag, 2002.
[28] J. Serra, *Image Analysis and Mathematical Morphology*, Academic Press, 1982.
[29] J.A. Sethian, "A Fast Marching Level Set Method for Monotonically Advancing Fronts," Proc. of National Academy of Science, vol.93, no.4, pp. 1591-1595, 1996.
[30] J.A. Sethian, *Level Set Methods and Fast Marching Methods*, second ed., Cambridge University Press, 1999.
[31] Y. Shi, P. Thompson, I. Dinov and A. Toga, "Hamilton-Jacobi Skeleton on Cortical Surfaces," IEEE Trans. Medical Imaging, vol.27, no.5, pp. 664-673, 2008.
[32] K. Siddiqi, S. Bouix, A. Tannebaum and S. Zucker, "Hamilton-Jacobi Skeletons," International Journal of Computer Vision, vol.48, no.3, pp. 215-231, 2002.
[33] K. Siddiqi and S. Pizer, *Medial Representations: Mathematics, Algorithms and Applications*, Springer, 2008.
[34] K. Siddiqi, A. Shokoufandeh, S. Dickinson and S. Zucker, "Shock Graphs and Shape Matching," International Journal of Computer Vision, vol.35, no.1, pp. 13-32, 1999.
[35] A.W. Toga and P.M. Thompson, "Mapping Brain Asymmetry," Nature Reviews Neuroscience, vol.4, no.1, pp. 37-48, 2003.
[36] C. Xu, T. Wang, Y.J. Liu, L. Liu and Y. He, "Fast Wavefront Propagation (FWP) for Computing Exact Geodesic Distances on Meshes," IEEE Trans. Visualization and Computer Graphics, DOI:10.1109/TVCG.2015.2407404, 2015.
[37] F.E. Wolter, *Cut Loci in Bordered and Unbordered Riemannian Manifolds*, PhD thesis, Technical University of Berlin, 1985.
[38] F.E. Wolter, *Cut Locus and Medial Axis in Global Shape Interrogation and Representation*, Design Laboratory Memorandum 92-2. MIT, 1993.